


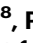


# Perinatal SSRI exposure impacts innate fear circuit activation and behavior in mice and humans

Received: 14 October 2024

Accepted: 28 March 2025

Published online: 06 May 2025

 Check for updates

Giulia Zanni<sup>1,2,9</sup>, Milenna T. van Dijk<sup>1,3,9</sup>, Martha Caffrey Cagliostro<sup>1,4</sup>, Pradyumna Sepulveda<sup>1</sup>, Nicolò Pini <sup>1,2</sup>, Ariel L. Rose<sup>1,2</sup>, Alexander L. Kesin<sup>1,2</sup>, Claudia Lugo-Candelas<sup>1,5</sup>, Priscila Dib Goncalves <sup>6</sup>, Alexandra S. MacKay <sup>1,2</sup>, Kiyohito Iigaya <sup>1,2,7,8</sup>, Praveen Kulkarni<sup>4</sup>, Craig F. Ferris <sup>4</sup>, Myrna M. Weissman <sup>1,3,6</sup>, Ardesheer Talati<sup>1,3</sup>, Mark S. Ansorge <sup>1,2</sup>  & Jay A. Gingrich<sup>1,2</sup>

Before assuming its role in the mature brain, serotonin modulates early brain development across phylogenetically diverse species. In mice and humans, early-life SSRI exposure alters the offspring's brain structure and is associated with anxiety and depression-related behaviors beginning in puberty. However, the impact of early-life SSRI exposure on brain circuit function is unknown. To address this question, we examined how developmental SSRI exposure changes fear-related brain activation and behavior in mice and humans. SSRI-exposed mice showed increased defense responses to a predator odor, and stronger fMRI amygdala and extended fear-circuit activation. Likewise, adolescents exposed to SSRIs *in utero* exhibited higher anxiety and depression symptoms than unexposed adolescents and also had greater activation of the amygdala and other limbic structures when processing fearful faces. These findings demonstrate that increases in anxiety and fear-related behaviors as well as brain circuit activation following developmental SSRI exposure are conserved between mice and humans. These findings have potential implications for the clinical use of SSRIs during human pregnancy and for designing interventions that protect fetal brain development.

Maternal anxiety and depression during pregnancy are associated with adverse offspring outcomes ranging from low birth weight to increased risk for psychopathology including anxiety and depression<sup>1–3</sup>. Affected mothers are typically prescribed selective serotonin reuptake inhibitors (SSRIs) to address these symptoms. Currently taken by ~6% of pregnant mothers<sup>4</sup>, their use during gestation is increasing<sup>5</sup>. While the

rationale for improving maternal mental health is clear, the impact of maternal SSRI use on the developing fetus remains understudied.

For the gestating fetus, SSRIs easily cross the placenta and block fetal serotonin (5-HT) reuptake<sup>6</sup>. The relative safety of SSRIs on fetal health has largely been assessed in the early postnatal period<sup>7</sup>. Only a few studies have attempted to assess whether in-utero SSRI exposure

<sup>1</sup>Department of Psychiatry, Vagelos College of Physicians and Surgeons, Columbia University, New York, NY, USA. <sup>2</sup>Division of Developmental Neuroscience, New York State Psychiatric Institute, New York, NY, USA. <sup>3</sup>Division of Translational Epidemiology, New York State Psychiatric Institute, New York, NY, USA. <sup>4</sup>Center for Translational Neuroimaging, Northeastern University, Boston, MA, USA. <sup>5</sup>Department of Child and Adolescent Psychiatry, New York State Psychiatric Institute, New York, NY, USA. <sup>6</sup>Department of Epidemiology, Mailman School of Public Health, Columbia University, New York, NY, USA. <sup>7</sup>Columbia Data Science Institute, Columbia University, New York, NY, USA. <sup>8</sup>Center for Theoretical Neuroscience, Zuckerman Institute for Mind Brain, and Behavior, Columbia University, New York, NY, USA. <sup>9</sup>These authors contributed equally: Giulia Zanni, Milenna T. van Dijk. ✉ e-mail: [ma2362@cumc.columbia.edu](mailto:ma2362@cumc.columbia.edu)

impacts offspring health later in life. While SSRI-exposure *in utero* may have few detrimental effects on human offspring at birth and in early infancy (but see refs. 8–10), some studies report cognitive and behavioral abnormalities in later childhood<sup>7,11,12</sup>. Likewise, several<sup>13–15</sup> but not all<sup>16,17</sup> epidemiological studies find that SSRI use in pregnancy is associated with depression and other psychiatric disorders in adolescent and young adult offspring. The apparently higher rate of offspring mental health issues as a result of gestational SSRI exposure comports with what has been reported in rodents<sup>18–23</sup>. However, the confounding factors complicating human epidemiological studies have cast doubt on whether similar developmental mechanisms are at play in each species.

The late-emerging effects of developmental SSRI exposure on human offspring outcomes are in line with rodent studies which suggest that the sequelae only manifest after sexual maturation<sup>24</sup>. The peak brain growth (along with peaking axonal and dendritic densities, monoamine levels, neurogenesis and gliogenesis) in rodents occurs in the first two postnatal weeks, which translates to the last trimester of human pregnancy<sup>25–28</sup>. Also, in rodents, 5-HT signaling is crucial to fetal brain development and plays a role in cell proliferation, neuronal differentiation, synaptogenesis, and neuronal migration<sup>29–31</sup>. Increases in 5-HT signaling during developmentally sensitive periods lead to altered structure and function throughout the brain in adult mice<sup>18–23,32</sup>. 5-HT is highly conserved across evolution<sup>33–35</sup>, yet it remains unclear whether SSRI exposure during early brain development exerts in humans the same effects seen in rodents. To better bridge between rodent and human studies, mechanistic insight is needed that functionally links developmental SSRI exposure to altered behavior in both mice and humans with the hypothesis that such functional changes should be conserved between species.

To address this hypothesis, we adopted a cross-species approach that harnesses the controlled experimental conditions of animal studies, while directly evaluating clinical relationships through a population study, within a single study framework. To this end, we exposed mice to predator odors while awake in an animal MRI machine and assessed the effect of early-life SSRI exposure on brain circuit activation and behavior. In parallel, we utilized the Adolescent Brain Cognitive Development Study<sup>36</sup> data of children who were subjected to emotionally laden (fearful) faces during an fMRI task and assessed the effect of in-utero SSRI exposure on brain circuit activation and behavior. By probing the circuitry of both mouse and human responses to ethologically relevant cues, we sought to determine whether similar brain-circuit effects of early SSRI exposure might be conserved across species. Our results demonstrate that early-life exposure to SSRIs indeed has conserved effects on innate fear circuit activation and behavior across phylogeny, suggesting shared mechanisms that will inform the public health implications of the broad usage of SSRI medications during pregnancy.

## Results

### PND2-11 fluoxetine increases innate freezing responses to a predator odor in adult mice

PND2-11 is a sensitive period in mice during which increased 5-HT signaling increases conditioned fear responses and anxiety in adulthood<sup>18,20</sup>. To increase translatability and establish fMRI compatibility, here we studied the effects of PND2-11 fluoxetine (PNFLX) versus saline (PNSAL) on innate fear responses to a predator odor (mountain lion urine) (Fig. 1A). On day 1 adult mice were habituated to an odor-attenuated chamber. During habituation, we found no significant differences in freezing behavior when comparing PNSAL to PNFLX animals (time x treatment interaction  $F_{1,22} = 0.4468$ ,  $p = 0.5108$ ; time effect  $F_{1,22} = 0.5761$ ,  $p = 0.4559$ ; treatment effect  $F_{1,22} = 0.668$ ,  $p = 0.4225$ ) (Fig. 1B). On day 2 mice were again placed into the testing apparatus and after 2 minutes predator odor was delivered. Two-way ANOVA analysis of freezing behavior revealed a significant interaction between treatment and predator odor ( $F_{1,22} = 4.794$ ,  $p = 0.0395$ ), a

significant effect of time ( $F_{1,22} = 46.98$ ,  $p < 0.0001$ ), and a significant effect of treatment ( $F_{1,22} = 7.956$ ,  $p = 0.01$ ) (Fig. 1C). Post-hoc analysis showed that PNSAL and PNFLX animals both increased freezing in response to the odor exposure ( $p = 0.0023$  PNSAL, and  $p < 0.0001$  PNFLX). However, PNFLX animals mounted a significantly higher freezing response when compared to PNSAL animals (post-odor PNSAL vs. PNFLX  $p = 0.001$ ). On day 2, PNFLX mice also had a lower latency to freeze during odor presentation compared to PNSAL animals (normalized to the latency to freeze on day 1,  $p = 0.032$ , Fig. 1C). Using a deep learning algorithm, deeplabcut (DLC) that automates animal pose estimation (Fig. 1E), we detected a significant main effects of predator odor on freezing ( $F_{1,22} = 9.783$ ,  $p = 0.0049$ , Fig. 1F) and speed ( $F_{1,22} = 10.19$ ,  $p = 0.0042$ , Fig. 1G). Post-hoc analysis showed that during the predator odor PNFLX animals freeze more than PNSAL ( $p = 0.0341$ ). Together our data demonstrate that adult PNSAL and PNFLX mice both mount a behavioral response to predator odor, but that the response is exacerbated after PND2-11 FLX exposure. A similar pattern was observed in adolescent PNFLX mice compared to PNSAL mice (Supplemental Fig. 1). Notably, there was no effect of treatment on fear responses to a neutral odor (Supplemental Fig. 2).

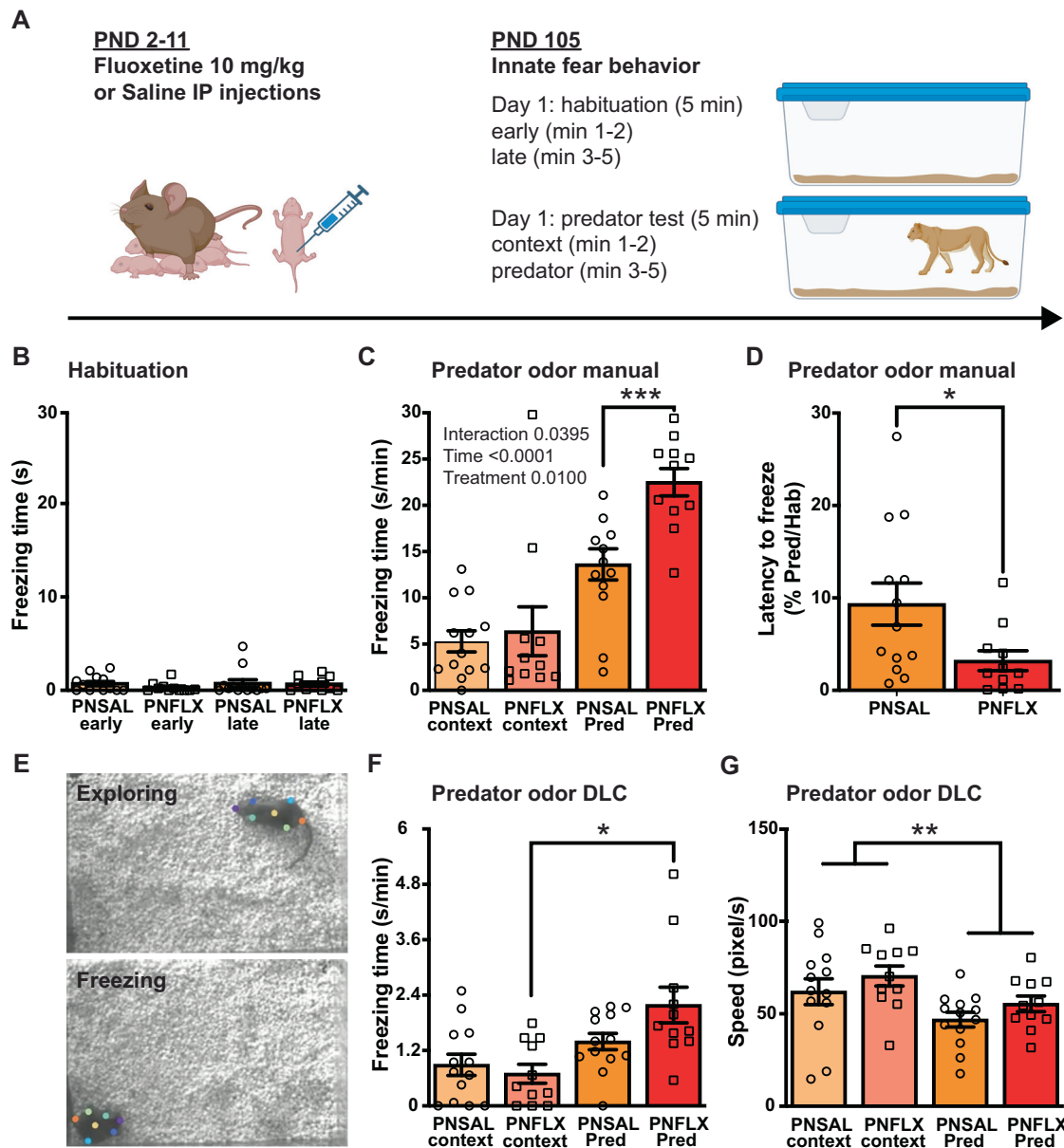
### PND2-11 fluoxetine increases BOLD response to predator odor in fear circuits

To address which brain regions are contributing to the SSRI-induced heightened innate fear response in mice we used fMRI to compare BOLD responses to predator odor in PNFLX mice and PNSAL controls (Fig. 2A). To elicit fear in awake mice we exposed animals to a predator odor in a mouse imaging holding system to which they were previously habituated to reduce motion artifacts<sup>37,38</sup>, and performed whole-brain imaging (Fig. 2B). The fMRI scans were registered to and analyzed using a 3-dimensional MRI mouse atlas with 134 bilateral segmented and annotated brain areas. Figure 2C and the table in Fig. 2D show the brain areas with a significant increase in positive BOLD volume of activation in response to predator urine odor in awake PNFLX mice compared to PNSAL mice (false discovery rate  $p = 0.0401$ ) in whole-brain analysis. These areas are ranked in order of their significance and out of the whole brain (134 areas) 28 brain areas showed significantly higher BOLD signals in PNFLX animals. Virtually all these areas belong to the previously described fear neural circuit (e.g., central and medial amygdala, periaqueductal gray, anterior cingulate cortex), that comprise the ascending reticular activating system involved in arousal (e.g., pedunculopontine tegmental area, medullary reticular area, and mesencephalic reticular formation), and regions broadly involved in emotional regulation (e.g., hypothalamus, putamen, and dorsal raphe). Exemplary fMRI time-courses from the central amygdala, mesencephalic reticular formation, and periaqueductal gray demonstrate the robust kinetics of the BOLD response to the odor exposure without an effect of treatment prior to odor administration (Supplemental Fig. 3). Overall, our data demonstrate that PND2-11 fluoxetine treatment leads to an exacerbated functional response to an innate fear stimulus across neural circuits involved in fear, arousal, and emotional regulation.

### Translation to human adolescent children from the ABCD study

In the rodents, fluoxetine was administered at PND2-11, corresponding to the third trimester *in utero* in humans<sup>27</sup>. Because behavioral consequences of prenatal SSRIs have been observed in adolescence<sup>10,15,39,40</sup>, we leveraged data from the ABCD study to test if our rodent findings translate to humans (Fig. 3A).

We selected children (Supplemental Table 3 for demographics) for whom 1) the biological mother was the reporter and had reported on medication use during pregnancy, 2) who had child behavior checklist (CBCL) scores at the two year follow-up wave (age 11-13 yo), 3) and complete covariate data (see “Methods”), resulting in  $N = 97$  SSRI+ children exposed to SSRIs *in utero* and  $N = 3876$  SSRI- unexposed children for analyzes without MRI data. Of this sample,  $N = 70$  SSRI+



**Fig. 1 | Postnatal fluoxetine (PND2-11) increases freezing to a predator.**

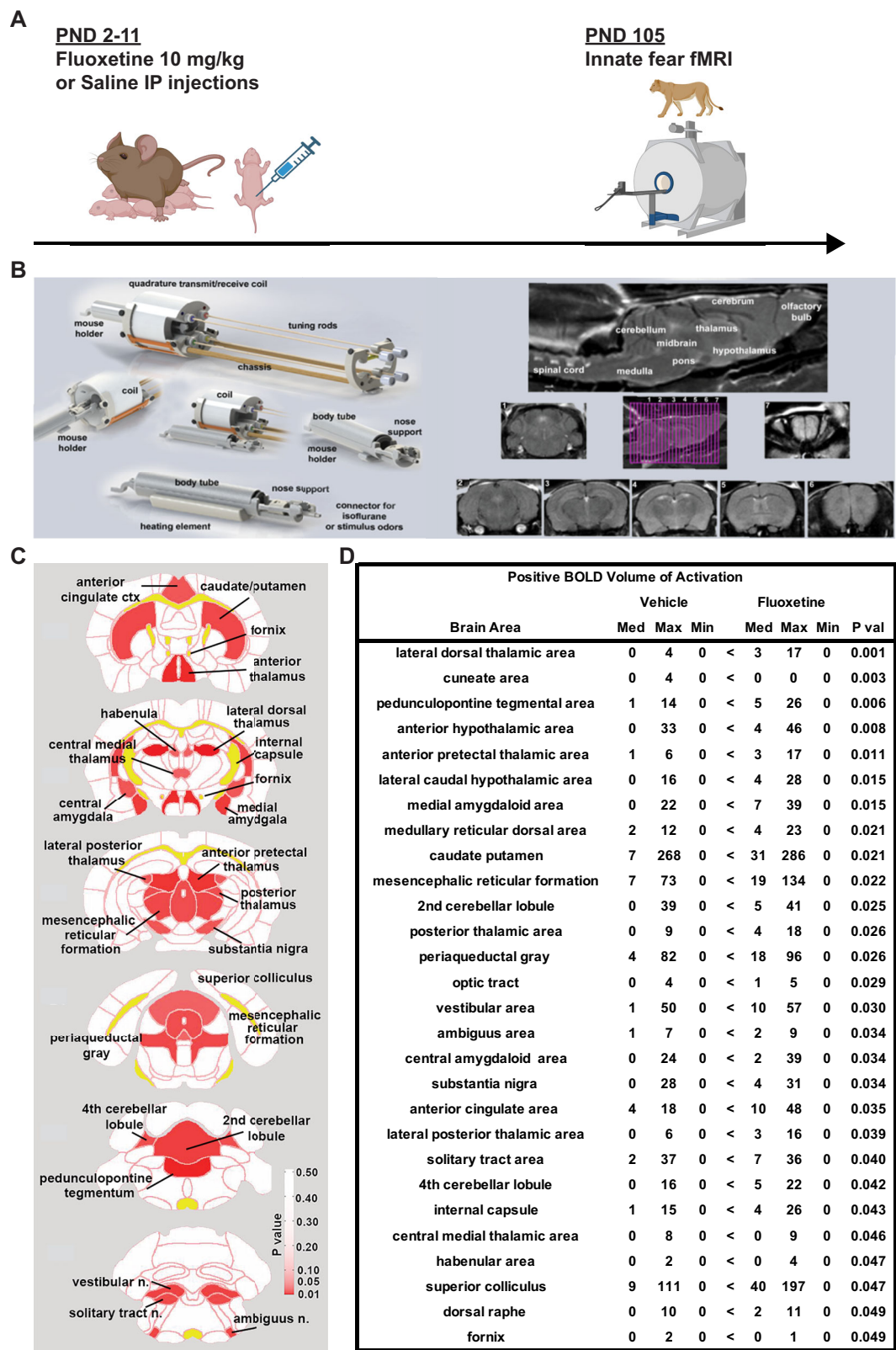
**A** Timeline of the adult mouse behavioral study. Created in BioRender. Zanni, G. (2025) <https://BioRender.com/m34p441>. **B** Manual freezing score during habituation early and late phases. **C** Manual freezing score during context re-exposure and during predator odor. **D** Latency to freeze expressed as percent change of habituation freezing latency. **E** Labeling of different animal body parts: nose (purple), tail base (orange), right ear (electric blue), left ear (cyan), right hip (blue), left hip

(light blue), mid back (yellow). Top picture shows animals exploring and the bottom picture shows an animal freezing. **F** DeepLab Cut freezing score during context re-exposure and during predator odor. **G** DeepLab Cut speed scoring during context re-exposure and during predator odor. Data are presented as mean values  $\pm$  SEM. Statistical tests used: ANOVA and Fisher's LSD posthoc. PNSAL  $N = 13$ , PNFLX  $N = 11$ . \* $p < 0.05$ ; \*\* $p < 0.01$ ; \*\*\* $p < 0.001$ . Source data are provided as a Source Data file.

children exposed to SSRIs *in utero* and  $N = 2989$  SSRI unexposed children had MRI data available and were used for the analyses containing MRI. All analyses used propensity score weighting as well as covariates, including maternal lifetime depression and current maternal anxiety and depressive symptoms, to mitigate potential confounding factors between (children of) mothers who were treated with SSRIs and those who were not (see “Methods”).

We first found that *in utero* SSRI exposure was associated with increased anxiety ( $b = 0.79$ ,  $p_{FDR} = 2.06 \times 10^{-18}$ ,  $p_{bonf} = 2.06 \times 10^{-18}$ ; standardized betas denote the predicted amount of standard deviations the outcome changes with SSRI exposure), depressive symptomatology ( $b = 0.43$ ,  $p_{FDR} = 2.26 \times 10^{-7}$ ,  $p_{bonf} = 6.77 \times 10^{-7}$ ), internalizing ( $b = 0.48$ ,  $p_{FDR} = 7.86 \times 10^{-10}$ ,  $p_{bonf} = 1.57 \times 10^{-9}$ ), and externalizing

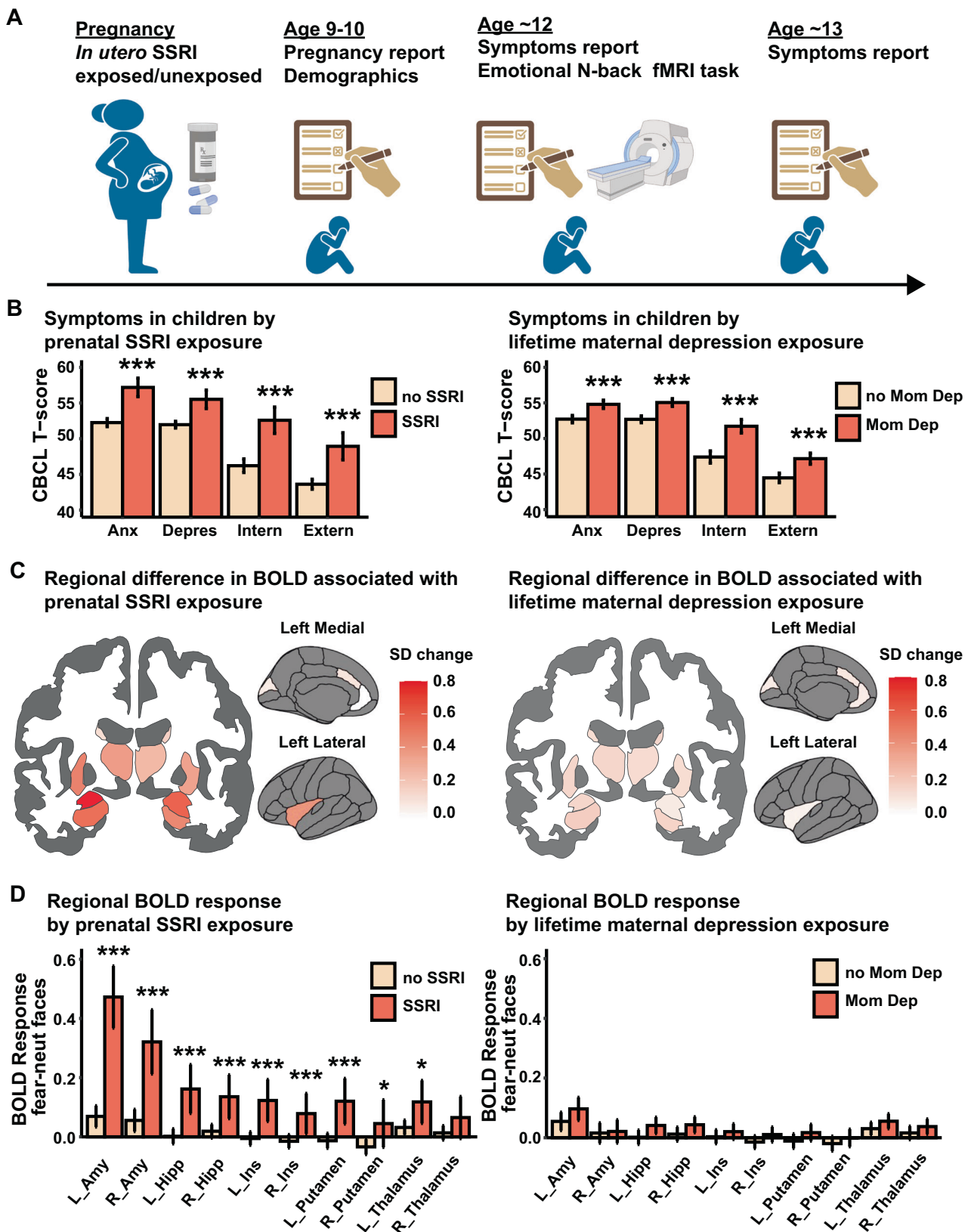
( $b = 0.24$ ,  $p_{FDR} = 0.002$ ,  $p_{bonf} = 0.007$ ) behavior at age 11–13 (Fig. 3B). As expected from extensive literature showing that maternal depression increases risk for psychiatric disorders in the offspring<sup>41,42</sup>, maternal lifetime depression as a covariate in the same model was also significant, but with smaller effect sizes as indicated by the betas, for anxiety ( $b = 0.13$ ,  $p_{FDR} = 0.006$ ,  $p_{bonf} = 0.018$ ), depressive symptoms ( $b = 0.15$ ,  $p_{FDR} = 1.43 \times 10^{-3}$ ,  $p_{bonf} = 2.86 \times 10^{-3}$ ), internalizing ( $b = 0.18$ ,  $p_{FDR} = 1.89 \times 10^{-5}$ ,  $p_{bonf} = 1.89 \times 10^{-5}$ ) and externalizing ( $b = 0.08$ ,  $p_{FDR} = 0.055$ ,  $p_{bonf} = 0.22$ ) behavior. Within the same sample, a model with maternal lifetime depression as the predictor and without prenatal SSRI use or maternal anxiety and depressive symptoms at time of child assessment as covariates, also resulted in significant associations with child anxiety ( $b = 0.33$ ,  $p_{FDR} = 8.44 \times 10^{-13}$ ,  $p_{bonf} = 2.53 \times 10^{-12}$ ),



**Fig. 2 | Postnatal fluoxetine (PND2-11) increases innate fear circuit activation.**  
**A** Timeline of the adult mouse fMRI study. Created in BioRender. Zanni, G. (2025) <https://BioRender.com/s15z123>. **B** Shown are the different components of the mouse imaging system. Below are sagittal and axial views of an awake mouse brain. Note the linearity along the Z-axis. The axial images taken from a 22-slice RARE sequence (0.6 mm thickness) demonstrate complete brain coverage from the olfactory bulbs to the brainstem. **C** Statistical map displaying relative positive BOLD

signal in response to predator urine odor in awake PNFLX compared to PNSAL mice. PNSAL N = 18, PNFLX N = 26. **D** List of significant brain areas, such as thalamus, putamen, brainstem and cerebellum, central amygdala, substantia nigra, periaqueductal gray, raphe, and habenula ranked in order of their significance in red for change in positive BOLD volume of activation (number of voxels) in PNFLX compared to PNSAL (false discovery rate  $p = 0.0401$ ). Statistical test used: Wilcoxon rank sum test corrected for multiple (134) comparisons.





depressive symptoms ( $b = 0.38$ ,  $p_{FDR} = 5.43 \times 10^{-17}$ ,  $p_{bonf} = 1.09 \times 10^{-16}$ ), internalizing ( $b = 0.40$ ,  $p_{FDR} = 5.79 \times 10^{-23}$ ,  $p_{bonf} = 5.79 \times 10^{-23}$ ) and externalizing ( $b = 0.25$ ,  $p_{FDR} = 5.01 \times 10^{-10}$ ,  $p_{bonf} = 2.01 \times 10^{-9}$ ) behavior (Fig. 3B), again showing maternal depression is associated with child outcomes but to a lesser degree than SSRI use according to the standardized coefficients.

To test brain activity associated with an innate fear response, we compared BOLD response to fearful versus neutral faces in SSRI<sup>+</sup> versus SSRI<sup>-</sup> children. Initially, in a hypothesis driven approach, we a priori selected seven regions of interest that have been associated with fear circuit activation<sup>43,44</sup>, and which we found to have enhanced activation in SSRI-exposed mice during innate fear (Fig. 2: amygdala,

**Fig. 3 | Effects of *in utero* SSRI exposure in human adolescents.** **A** The experimental timeline. At baseline mothers reported on their pregnancy and demographics. Children underwent an MRI scan approximately two years post-baseline, and mothers filled out the Child Behavioral Checklist (CBCL) to assess symptoms at that time and one year post-MRI. Created in BioRender. Zanni, G. (2025) <https://BioRender.com/e26b462>. **B Left.** *In utero* SSRI exposure is associated with increased CBCL symptoms, accounting for maternal lifetime depression and maternal anxiety and depressive symptoms. N = 97 SSRI<sup>+</sup>, N = 3876 SSRI<sup>-</sup>. **Right.** Maternal lifetime depression is also associated with increased offspring symptoms. **C Left.** *In utero* SSRI exposure is associated with increased amygdala, hippocampus, insula, putamen and thalamus activation to fearful-neutral faces, depicted as

change in standard deviation of the BOLD response accounting for maternal lifetime depression and maternal anxiety and depressive symptoms. **Right.** Exposure to maternal lifetime depression does not result in significant differences in BOLD response to fearful-neutral faces. **D** Same analysis as (C) depicted as predicted means by group. N = 70 SSRI<sup>+</sup>, N = 2989 SSRI<sup>-</sup>. **Left.** *In utero* SSRI exposure is associated with increased BOLD activation to fearful-neutral faces. **Right.** Exposure to maternal lifetime depression does not result in differential BOLD response. Linear mixed effects models with propensity score weighting, 2-tailed, FDR-corrected. Error bars signify 95% confidence intervals. Precise p-values are reported in the main text. \**p* < 0.05; \*\*\**p* < 0.005.

**Table 1 | Left and right amygdala activity in response to fearful vs neutral faces predicts concurrent and future depressive symptomatology**

Predictor	Outcome	At time of MRI			1 year post MRI		
		St. Beta	P <sub>FDR</sub>	P <sub>BONF</sub>	St. Beta	P <sub>FDR</sub>	P <sub>BONF</sub>
Left Amygdala	Anxiety symptoms	0.12	2.78 × 10 <sup>-7</sup>	8.33 × 10 <sup>-7</sup>	-0.01	0.69	1
	Depressive symptoms	0.11	1.86 × 10 <sup>-8</sup>	3.71 × 10 <sup>-8</sup>	0.05	0.024	0.049
	Internalizing Symptoms	0.06	3.98 × 10 <sup>-4</sup>	1.99 × 10 <sup>-3</sup>	-0.004	0.79	1
	Externalizing Symptoms	0.004	0.83	1	-0.01	0.63	1
Right Amygdala	Anxiety symptoms	0.07	1.22 × 10 <sup>-3</sup>	7.34 × 10 <sup>-3</sup>	0.01	0.63	1
	Depressive symptoms	0.12	1.86 × 10 <sup>-8</sup>	2.54 × 10 <sup>-8</sup>	0.08	1.87 × 10 <sup>-4</sup>	1.87 × 10 <sup>-4</sup>
	Internalizing Symptoms	0.08	7.97 × 10 <sup>-7</sup>	3.19 × 10 <sup>-6</sup>	0.02	0.63	1
	Externalizing Symptoms	-0.02	0.41	1			

rostral and caudal ACC, cuneus, thalamus, caudate and putamen) as well as two regions that were affected in previous rodent or infant developmental SSRI studies (hippocampus and insula)<sup>45-47</sup>. Similar to our findings in mice, SSRI<sup>+</sup> children had increased response to fearful-neutral faces in the bilateral amygdala (left: *b* = 0.76, *p*<sub>FDR</sub> = 2.6 × 10<sup>-14</sup>, *p*<sub>BONF</sub> = 2.6 × 10<sup>-14</sup>; right: *b* = 0.51, *p*<sub>FDR</sub> = 2.07 × 10<sup>-6</sup>, *p*<sub>BONF</sub> = 4.14 × 10<sup>-6</sup>; Fig. 3C, D), bilateral hippocampus (left: *b* = 0.45, *p*<sub>FDR</sub> = 3.60 × 10<sup>-6</sup>, *p*<sub>BONF</sub> = 1.08 × 10<sup>-5</sup>; right: *b* = 0.33, *p*<sub>FDR</sub> = 2.82 × 10<sup>-4</sup>, *p*<sub>BONF</sub> = 1.69 × 10<sup>-3</sup>), bilateral insula (left: *b* = 0.41, *p*<sub>FDR</sub> = 3.20 × 10<sup>-5</sup>, *p*<sub>BONF</sub> = 1.28 × 10<sup>-4</sup>; right: *b* = 0.29, *p*<sub>FDR</sub> = 0.003, *p*<sub>BONF</sub> = 0.021), bilateral putamen (left: *b* = 0.38, *p*<sub>FDR</sub> = 7.02 × 10<sup>-5</sup>, *p*<sub>BONF</sub> = 3.51 × 10<sup>-4</sup>; right: *b* = 0.25, *p*<sub>FDR</sub> = 0.014, *p*<sub>BONF</sub> = 0.121) and left thalamus (*b* = 0.26, *p*<sub>FDR</sub> = 0.012, *p*<sub>BONF</sub> = 0.095), but not in ACC, caudate, or cuneus. These findings, except for left thalamus and right putamen, remained significant when accounting for concurrent child CBCL scores (Supplemental Table 4). In an unbiased whole brain analysis, BOLD response to fearful-neutral faces, was again significantly stronger in the amygdala, hippocampus, putamen, and insula after *in utero* SSRI exposure (Supplemental Table 5). Additionally, the whole brain analysis also revealed increased activation in temporal regions, ventral diencephalon, and brain stem. The latter two may match our rodent findings of increased activity in the hypothalamus and substantia nigra (ventral diencephalon), and periaqueductal gray (brain stem), but differences in brain atlas resolution between mouse and human do not allow us to conclude this matching unequivocally.

Maternal lifetime depression was controlled for as a covariate in these models and was significantly associated with bilateral cuneus and thalamus BOLD responses. However, after FDR correction for multiple comparisons maternal lifetime depression did not remain significantly associated with BOLD response in any region. In a model without covariates for prenatal SSRI exposure and maternal anxiety and depressive symptoms at time of MRI, maternal lifetime depression was not significantly associated with BOLD response to fearful-neutral faces in any region after FDR correction (Fig. 3C,D and Supplemental Table 6). To further isolate SSRI effects from maternal depression effects, we tested whether prenatal SSRI use was also associated with differential BOLD response within the

subset of children of mothers who reported having a lifetime history of depression (N = 45 SSRI<sup>+</sup> children of mothers with lifetime depression and N = 670 SSRI<sup>-</sup> children of mothers with lifetime depression). In children of mothers with lifetime depression, prenatal SSRI use remained associated with amygdala response (left: *b* = 0.74, *p*<sub>FDR</sub> = 8.81 × 10<sup>-6</sup>, *p*<sub>BONF</sub> = 8.81 × 10<sup>-6</sup>; right: *b* = 0.30, *p* = 0.047, *p*<sub>FDR</sub> = 0.28) and marginally left hippocampal response (left: *b* = 0.32, *p* = 0.008, *p*<sub>FDR</sub> = 0.076). A last sensitivity analysis comparing three groups: 1) children exposed to SSRI *in utero*, 2) children exposed to maternal lifetime depression who did not take SSRIs during pregnancy, 3) non-exposed children also shows that the SSRI-exposed group had increased BOLD response (Supplemental Table 7), again suggesting specificity of the SSRI exposure effects.

When including interactions with sex into the models to investigate sex differences, we find that increased symptoms and BOLD response to fearful stimuli are predominantly present in SSRI-exposed girls (Supplemental Results and Table S8-12).

Lastly, controlling for prenatal SSRI use and maternal lifetime depression as well as the other covariates, bilateral amygdala response was associated with child anxiety, depressive symptomatology and internalizing, but not externalizing behavior at time of MRI (Table 1). Right amygdala response was associated with future depressive symptoms one year post MRI (N = 64 SSRI<sup>+</sup>, N = 2664 SSRI<sup>-</sup> with follow-up data; Table 1). Furthermore, left (but not right) amygdala response to fearful-neutral faces formally mediated the response between SSRI exposure and anxiety symptoms at time of MRI (indirect effect: 0.014, *p* < 0.0001; total effect: 0.14, *p* < 0.0001, proportion mediated: 9.3% *p* < 0.0001), suggesting heightened amygdala activity is part of the mechanism that leads from SSRI exposure to increased anxiety.

These findings show that similar to the rodent findings, *in utero* SSRI exposure is associated with increased symptomatology, increased fear circuit-related brain activation to innately fearful stimuli and that the amygdala predicts current as well as future depressive symptomatology, suggesting that the amygdala mediates effects by which prenatal SSRI exposure leads to increased risk for psychopathology in the offspring.

## Discussion

The present findings demonstrate that elevated 5-HT signaling during early development increases neurobiological and behavioral innate fear responses later in life in both mice and humans. In mice, our behavioral findings add to the wide-ranging consequences observed after PND2–11 SSRI exposure, including reduced motivation, increased anxiety-like behavior, impaired fear extinction, and increased depressive-like behaviors in adulthood<sup>18,20,48–50</sup>. Importantly, these phenotypes in mice align well with the increased anxiety, depression, internalizing as well as externalizing symptoms following *in utero* SSRI exposure we observed here in human adolescents. The overlap in amplified innate fear circuit activation between mice and humans suggests highly evolutionarily conserved mechanisms of serotonin sensitivity during late gestation and early postnatal brain development.

Insight into possible mechanisms underlying altered behavior and fear circuit activation after developmental SSRI exposure comes predominantly from mouse studies. Mice exposed to early-life SSRIs exhibit reduced innervation of the medial prefrontal cortex (mPFC) by 5-HT fibers<sup>18</sup> possibly resulting in reduced mPFC top-down inhibition of the amygdala underlying exaggerated freezing responses in fear conditioning<sup>51–53</sup>. Moreover, we have found in mice that neurons in the infralimbic and prelimbic areas of the PFC exhibit altered firing properties after early-life SSRI exposure, again providing a link to altered top-down control of amygdala function<sup>18</sup>. Similarly, mice with early-life genetic loss of 5-HT transporter function have less 5-HT innervation of the amygdala and consequently less direct serotonergic inhibitory influence via 5-HT<sub>1A</sub> receptors in this structure<sup>21,54</sup>.

We can speculate that similar mechanisms may be operative in the developing human fetus. However, there have been no studies that have attempted to examine the density of 5-HT innervation in human brain structures after *in utero* SSRI exposure. Furthermore, rodents and higher primates both demonstrate widespread transient expression of the 5-HT transporter in non-serotonergic neurons during the mid-gestation and into early infancy<sup>55–59</sup>. We have hypothesized that the period of development sensitive to 5-HT blockade in humans also overlaps both the maturation of 5-HT axon arborization and the period of transient expression of 5-HTT in non-serotonergic structures. Hyperactivity in amygdala and insula could be a consequence of early structural changes in amygdala and insula volume and connectivity observed in human neonates<sup>45</sup> and childhood<sup>39</sup> exposed to *in utero* SSRIs. Thus, in analogy to our mouse-hypothesis, *in utero* SSRI exposure in humans may affect fear circuitry function and psychopathology by decreasing top-down control<sup>60</sup>. Indeed, hyperactivity in the insula-amygdala circuit is associated with (increased risk for<sup>61</sup>) anxiety disorders<sup>62</sup> which comports with the increased internalizing symptoms observed in SSRI-exposed children in our study. Importantly, amygdala reactivity to faces has been associated with future response to antidepressant medication<sup>63</sup>.

It is important to note that some brain regions were differentially activated in mice and humans, i.e., mouse cuneate, human insula, and human temporal structures. These differences could stem from the olfactory versus visual stimuli used in the mouse and human task, respectively. Alternatively, these differences could be the consequence of divergent brain evolution between mice and humans.

In summary, we have identified an evolutionarily conserved effect of 5-HTT blockade on fear circuit activation in response to innate fear cues later in life. Our experimental mouse model can control for confounding factors, such as maternal depression, comorbidities, and socioeconomic status (that typically confound the interpretation of human observational data), and thereby allows for experimental designs that can establish causality. Mouse to human translation is hardly ever one to one. Yet, parallel translation to humans shows that our findings are clinically relevant and ethologically valid. Our findings

across ages furthermore suggest that effects of perinatal SSRI exposure are present in adolescence and persist through adulthood.

Prenatal anxiety and depression adversely affect both mother and child and motivate the public health efforts to identify and treat these disorders. SSRIs are a common therapeutic strategy in perinatal maternal emotional disorders, however the present cross-species data and prior studies on single species<sup>4,45,64,65</sup> indicate that we need more mechanistic understanding of how pharmacological factors like SSRIs impact early brain development and later result in maladaptive behaviors. In turn this knowledge will enable the development of more effective treatments that better support the mother and the developing fetus.

## Methods

### Mouse study

**Ethical permission guidelines and subjects.** Pet1Cre mice on a 129SvEv/Tac background were bred at Columbia Psychiatry, New York State Psychiatric Institute. All methods were approved by the Animal Care and Use Committee of the New York State Psychiatric Institute and in accordance with the NIH Guide for the Care and Use of Laboratory Animals according to IACUC protocol number 1562. Mice used for experiments were born from litters containing 2–10 pups. Mice were separated by sex and weaned into groups of five mice per cage at P26. Animals were maintained on a 12/12 h light/dark cycle (lights on at 7:00 a.m.) and provided with food and water *ad libitum*. During the perinatal period, postnatal day 2 to 11 (PND 2–11) mice received daily intraperitoneal injections with either vehicle saline (PNSAL; 0.9% NaCl, 5 ml/kg) or fluoxetine (PNFLX; 10 mg/kg in VEH, 5 ml/kg). This dose paradigm in mice produced therapeutically relevant blood levels  $360 \pm 123$  ng/ml in the pups without gross changes in viability and growth<sup>20</sup>. Multiple cohorts of mice were created for the various experiments. For innate fear behavioral assessment, we used female and male mice from at least 4 litters and 7 individuals in each treatment group. For adolescent fear behavior we used Pet1Cre mice on a 129SvEv/Tac background (Male PNSAL  $n = 4$ , Male PNFLX  $n = 6$ , Female PNSAL  $n = 8$ , Female PNFLX  $n = 5$ ). For adult fear behavior we used Pet1Cre mice on a 129SvEv/Tac background (Male PNSAL  $n = 4$ , Male PNFLX  $n = 6$ , Female PNSAL  $n = 9$ , Female PNFLX  $n = 5$ ). For fMRI experiments we used Male PNSAL  $n = 8$ , Male PNFLX  $n = 13$ , Female PNSAL  $n = 10$ , Female PNFLX  $n = 13$ .

**Innate fear behavior.** Adult mice were handled for a week prior to testing to get acquainted with the experimenter. Innate fear behavior was tested on two consecutive days: habituation and test.

**Fear apparatus in adulthood.** On the day of testing animals were brought individually into the behavior room in a transport cage. The testing apparatus consisted of an air-tight clear plastic chamber that has a clear lid ( $12 \frac{1}{2}$  "L  $\times$   $8 \frac{1}{2}$  "W  $\times$   $8 \frac{1}{2}$  "H). The animals were tested individually for 5 minutes during habituation and allowed to explore the chamber maze. On the following day the animals were tested for 5 minutes in presence of a predator odor. The predator odor consisted of mountain lion urine (LLC 92012) that was delivered in an odor-attenuated air flow-controlled chamber. Briefly, predator odor air or odor-free air was administered via a stopcock valve connected two Erlenmeyer flasks via different tubing lines. The odor was introduced in the chamber by placing a piece of filter paper scented with predator odor (500  $\mu$ l) at the top of the flask connected with the odor delivery line. Continuous airflow was maintained through the airtight chamber at 4 psi via calibration columns. The fear odor experiment was performed under a laminar flow hood and airflow was exhausted from the building.

**Fear testing in adolescence.** On the day of testing animals were brought individually into the behavior room in a transport cage. The

testing apparatus was the same as above. A predator-like odor, 2-methyl-2-thiazoline (2MT), was delivered in an odor-attenuated air flow-controlled chamber. We used 2MT because it has consistent formulation and high potency, and this odor has been previously shown to induce measurable levels of fear-like behaviors in mice amounting to 80–90% freezing<sup>66–68</sup>. The testing started with 2 minutes of odor-less air followed by 3 minutes of 2MT, and 10 more minutes of odor-less air (Supplemental Fig. 1).

**Manual behavioral scoring and video analysis.** A top view camera (Digital USB 2.0 CMOS Camera, DMK 22AUC03) was connected to the ANYmaze software and the animal's body was tracked throughout habituation and test tasks in both exposures. All videos in adulthood and adolescence were analyzed offline using ANYmaze software. The parameters included in the ANYmaze analysis were total time freezing (3 seconds immobility threshold), total distance traveled, and latency to immobility. For manual scoring we used the key function of ANYmaze and freezing was visually observed as pausing of all mouse activity including head movement that the automated scoring is not able to reliably capture. We analyzed early phases during habituation corresponding to minute 1–2, and late phases from min 3–5. During predator odor we measure freezing responses to the same habituation context re-exposure from minute 1–2 and during predator odor from minutes 3–5.

**DeepLabCut tracking analysis.** We conducted a more granular analysis of the adult innate fear behavioral response in our animal model using DeepLabCut (DLC)<sup>69</sup>. This software enables estimation of poses by tracking the animal body parts with high accuracy. Data was recorded at 15 Hz by one camera: the 640 × 480 pixels images were acquired with a Digital USB 2.0 CMOS Camera, DMK 22AUC03. Since our behavior was uniform overtime, we extracted 280 labels using K-Means clustering and two independent human annotators blinded to the treatment were trained to localize the following body parts: nose, left and right ear, left and right hip, tailbase, and midback. The tracking consisted of randomly extracted frames for a total of 20 frames from 14 mice scored separately for habituation and predator odor. We then created a training dataset using a resnet\_50 network and default augmentation method. To train the network we used a shuffle=1, training index=0, and a 150k maximum iterations, the point at which the training reached a plateau. To validate the manual scoring of speed and freezing, we used custom Python scripts to analyze the DLC output files (csv array with x/y coordinates and likelihood values for each body part)<sup>70</sup>. We preprocessed the position data to correct loss of tracking of animal body parts. We removed body parts with unrealistic placements (i.e., with a Euclidean distance larger than the mouse body, ~200 pixels, from the rest of the body parts) and linearly interpolated their position with the positions obtained from contiguous frames. We estimated the animals' speed using the Euclidean distance of the mid back position between frames. The speed time series was smoothed individually using a moving average filter (15 points).

To estimate freezing time, the 10th percentile of the speed distributions along the entire session was selected as threshold for each individual animal. Any period with at least 15 contiguous samples (i.e., 1 s) under the threshold was set as freezing time. We defined the habituation period as 100 ms–2000 ms and the predator period as 2000 ms – 5000 ms relative to the beginning of the recording. We skipped the early frames since those labels had low likelihood values, indicating that the mouse was not present in the arena yet. If no freezing time was identified between the beginning of the habituation period (100 ms) and the end of the predator period (5000 ms), the speed threshold was individually incremented. The threshold was incremented in steps of 5 percentiles until the freezing time across habituation and predator periods was at least 60 frames (4 seconds).

## Functional magnetic resonance imaging (fMRI) during predator odor exposure

**Awake Mouse Imaging System.** Presented in Fig. 1A are the different components of the mouse imaging system showing a radiofrequency coil and MR compatible restraining system for imaging awake mice (Ekam Imaging, Boston MA USA). As previously described the awake mouse imaging system can reliably detect BOLD signal changes irrespective of baseline changes between unacclimated and acclimated animals<sup>38</sup>. The quadrature transmit/receive volume coil (ID 38 mm) provides excellent anatomical resolution, signal-noise-ratio (SNR) for voxel-based BOLD fMRI. The unique cushioned helmet design of the holder essentially stabilizes the head in a cushion, minimizing any discomfort normally caused by ear bars and pressure points used to immobilize the head for awake animal imaging<sup>71</sup>. Odorants are delivered through PE tubing connected to a nose cone built into the tubular bite bar used to secure the front incisors of the mouse in the head holder. A movie showing the set-up of a mouse for awake imaging is available at <http://www.youtube.com/watch?v=W5Jup13isqw>.

**Acclimation.** A week prior to the first imaging session, all mice were acclimated to the imaging system with the head restraint and sounds typical of the scanner. Mice were secured into their holding system while anesthetized with 1–2% isoflurane. Following cessation of isoflurane, fully conscious mice were put into a 'mock scanner' (a black box with audio of MRI pulses) for 30 minutes for four consecutive days. Acclimation in awake animal imaging significantly reduces physiological effects of the autonomic nervous system including heart rate, respiration, corticosteroid levels, and motor movements helping to improve contrast-to-noise and image quality<sup>37,38</sup>. For some experiments, acclimation training for 10–14 days is likely ample under certain conditions<sup>72</sup>. In our experience 4 days has been sufficient<sup>37,71</sup> and here we did not detect movement artefacts that would indicate treatment-specific flight or freezing responses.

**Imaging acquisition and pulse sequence.** Experiments were conducted using a Bruker Biospec 7.0 T/20-cm USR horizontal magnet (Bruker, Billerica, Massachusetts) and a 20-G/cm magnetic field gradient insert (ID = 12 cm) capable of a 120- $\mu$ s rise time (Bruker)<sup>73</sup>. At the beginning of each imaging session, a high-resolution anatomical data set was collected using the RARE pulse sequence (20 slice; 0.75 mm; FOV 2.5 cm; data matrix 256 × 256; repetition time (TR) 2.1 sec; echo time (TE) 12.4 msec; Effect TE 48 msec, NEX 6; 6.5 min acquisition time). Functional images were acquired using a multi-slice HASTE pulse sequence (Half Fourier Acquisition Single Shot Turbo Spin Echo). With this sequence it is possible to collect twenty, 0.75 mm thick, axial slices in less than six seconds. With a FOV of 2.5 cm and a data matrix of 96 × 96, the in-plane pixel functional resolution for these studies was 260  $\mu$ m<sup>2</sup>.

**Provocation paradigm - odor stimulant.** Awake adult mice were imaged for changes in BOLD signal intensity in response to the odor of mountain lion urine (PredatorPee Liquid, [www.predatorpee.com](http://www.predatorpee.com)). Scans consisted of two epochs: a 4 min "baseline" epoch and an 8 min "stimulus presentation" epoch for a total of 12 min. In the custom-designed head restraint described above, the bar that holds the incisors in place functions simultaneously as an odor delivery tube. The odor delivery tube is connected by polyethylene tubing to an aquarium pump located outside the magnet room. During baseline, all subjects were presented with ambient air at a flow rate of approximately 1.5 lpm. At the start of stimulus presentation, sealed plastic cups containing the odor (15 $\mu$ L mountain lion urine on a cotton ball) were placed into the flow stream. Following each subject's imaging session, all imaging components were thoroughly cleaned and sanitized, and a minimum 10-minute odor clearance period was allowed between subjects for any residual odor to dissipate. Charcoal odor



capture canisters were additionally placed around the room to further aid in clearance of olfactory stimuli.

**Image analysis.** Images were aligned and registered to a 3D mouse brain atlas, which is segmented and labeled with 134 discrete anatomical regions (Ekam Solutions, Boston MA). The alignment process was facilitated by an interactive graphic user interface. The following parameters were applied: Quality: 0.97, Smoothing: 0.35 mm, Separation: 0.50 mm. Gaussian smoothing was performed with a Full Width at Half Maximum (FWHM) of 0.8 mm. The registration process involved translation, rotation and scaling independently and in all three dimensions. Matrices that transformed each subject's anatomy were used to embed each slice within the atlas. All pixel locations of anatomy that were transformed were tagged with major and minor regions in the atlas. This combination created a fully segmented representation of each subject within the atlas. The inverse transformation matrix [Ti]-I for each subject (i) was also calculated.

In voxel-based analysis, the BOLD % change of each independent voxel was averaged for all subjects. It is a sensitive and robust analysis method that can detect not only changes in signal intensity but also in number of activated voxels within an ROI, thus differences in spread of activation<sup>38,74,75</sup>. Statistical t-tests were performed on each voxel (ca. 15,000 in number) of each subject within their original coordinate system with a baseline threshold of 1% BOLD change to account for normal fluctuation of BOLD signal in the awake rodent brain<sup>76–78</sup>. To address the multiple t-tests conducted, a mechanism for controlling false-positive detections was introduced<sup>79,80</sup>, to ensure that, on average, the false-positive detection rate remained below 0.05. The formula used was:

$$P_i \leq i/V q/c(V)$$

Where  $P_i$  is the p-value from the t-test at the  $i$ -th pixel within the region of interest (ROI) containing  $V$  pixels, each ranked based on its probability value. The false-positive filter value  $q$  was set to 0.2 for our analysis, and the predetermined constant  $c(V)$  was set to unity<sup>81</sup>, providing conservative estimates for significance. Pixels that were statistically significant retained their relative percentage change values, while all other pixel values were set to zero. A 95% confidence level, two-tailed distributions, and heteroscedastic variance assumptions were employed for the t-tests. The median number of activated voxels in each of the 134 regions between the PNSAL group and PNFLX group were compared using a Wilcoxon rank sum test and results were corrected for multiple comparisons using false discovery rate for 134 comparisons.

**Statistical analyses—mouse study.** Data were analyzed using GraphPad Prism (version 8.4.3). Two-way ANOVA were used for analysis of variance of Treatment (vehicle vs perinatal fluoxetine), Exposure (habituation vs test), and Time variables. When interactions of variables were significant a multiple comparison post hoc test was conducted, and significance was reported in the graph. Significant main effects of individual variables were also reported in the graph. Outliers were identified using the ROUT method using a Q coefficient of 1% and the pairwise comparison was removed from the analysis. All data are presented as the mean  $\pm$  SEM. Significance was  $*p < 0.05$ ;  $**p < 0.01$ ;  $***p < 0.001$ .

## Human study

**ABCD study data and IRB ethical permission.** For the human experiments we did secondary analyses of Adolescent Brain Cognitive Development<sup>SM</sup> Study (ABCD Study<sup>®</sup>) data, a large longitudinal nationwide study of children recruited from primary and public-school systems at 21 sites nationwide. ABCD study procedures were approved by the Institutional Review Board at the University of California at San

Diego, San Diego, CA. Parents provided written informed consent; children provided verbal assent. The local New York State Psychiatric Institute and Columbia University IRB approved secondary analyses of ABCD data (ABCD Study ID 2008, <https://doi.org/10.15154/1528668>). Since phenotypes may only appear in adolescence<sup>40</sup>, we used the latest MRI data available, the two-year follow up data, when the children were 10.6–13.8 years old. The analysis sample was from the NDA's two year follow-up release (downloaded through October 2022) and had the following additional inclusion criteria: biological mother reporting, data available about prenatal medication use and other prenatal and birth history as well as full data on other covariates (see below) and two year follow-up data available from the parent-report child behavior checklist (CBCL), which resulted in  $N = 95$  SSRI<sup>+</sup> children exposed to SSRIs *in utero* and  $N = 3813$  SSRI<sup>-</sup> unexposed children. For analyses including an association with BOLD response we also required complete data on the N-BACK fMRI task including behavior and that MRI scans passed quality control measures as advised by the ABCD study, resulting in  $N = 68$  SSRI<sup>+</sup> children exposed to SSRIs *in utero* and  $N = 2928$  SSRI<sup>-</sup> unexposed children.

**Procedures and variables of interest.** Biological mothers completed reports on demographics, prenatal history, CBCL about their child, adult self-report (the equivalent to CBCL for adults, about themselves), and their own psychiatric history through the family history assessment (see Supplemental Table 12 for detailed variables).

**MRI.** As reported in detail elsewhere<sup>36</sup> children performed the emotional N-back task in the MRI scanner. Briefly, children viewed images of positive (happy), negative (fearful) or neutral emotional faces or pictures of places and indicated if the current image was the same as the previous image (0-back) or as the image they saw two images earlier (2-back). MRI images were acquired on one of three types of 3 T MRI scanners (Siemens Prisma, Phillips, General Electric 750) using multichannel coils (Casey et al., 2018). Image processing was standardized using a preprocessing pipeline implemented by the ABCD study, previously reported<sup>82</sup>. Briefly, after preprocessing which included motion correction, registration and normalization to the mean across time per voxel, task-related activation strength was estimated through subject-level general linear models using AFNI's 3dDeconvolve<sup>83</sup>. A gamma function and its temporal derivative were used to model the hemodynamic response. Beta coefficients and standard errors of the mean were mapped to FreeSurfer generated Regions of Interests (ROIs): cortical surface parcellations and sub-cortical segmentations. A weighted (a function of remaining images after motion correction) average across two runs was calculated for final mean beta weights and SEMs for each ROI and contrast. We used the mean beta weights for the contrast fearful compared to neutral faces, in a-priori selected regions of interest: amygdala, hippocampus, putamen, insula, rostral and caudal ACC, cuneus and thalamus. This contrast collapses over memory conditions, thus averaging out memory effects, and independently measures BOLD response to innately fearful stimuli compared to neutral stimuli, similar to the mouse study<sup>84</sup>. The regions were selected to translate the mouse findings (Fig. 2) and/or because in earlier work with neonatal infants<sup>45</sup> we had found that the amygdala and the insula were affected. However we also performed an unbiased whole-brain analysis including all available ROIs to ensure findings are similar regardless of approach (Supplemental Table 5)

## Measures

**Predictor: prenatal SSRI use.** Data regarding SSRI use once mothers knew that they were pregnant were used to make a composite SSRI use variable. Children were grouped as exposed to SSRI if mothers reported having used while they knew they were pregnant the following: fluoxetine, fluvoxamine, sertraline, citalopram, escitalopram,

and/or paroxetine, but did not also use other types of antidepressants such as bupropion, duloxetine, MAO-inhibitors, tricyclic antidepressants, anti-anxiety medication, opioids, antipsychotic medication, anti-convulsant medication, stimulants or sleep aids.

Because the SSRI exposure had the largest effect size on the amygdala response, we then selected bilateral amygdala BOLD response to fearful versus neutral faces as a predictor for symptomatology at time of MRI and at the 1 year time point after MRI (N = 2670 had this follow-up data available).

**Potential confounders.** All our analyzes controlled for birth weight, child age at the time of MRI, sex assigned at birth, puberty score at time of MRI, maternal lifetime depression, maternal depression and anxiety symptomatology at time of child MRI (ASR), maternal age at birth, maternal race/ethnicity, area deprivation index, maternal education, combined household income, birth complications, doctors visits during pregnancy, pregnancy illnesses, prenatal vitamin use, prematurity, whether the pregnancy was planned, delivery by cesarean, substance use knowing of pregnancy of the following substances: caffeine, tobacco, alcohol, cannabis and cocaine and crack cocaine, oxycodone. In addition, we added in random effects terms for MRI scanner site and family relatedness.

For analyzes concerning the emotional N-back fMRI task we additionally controlled for behavior on the task for neutral and fearful images (rate of correct responses and reaction time). We performed sensitivity analyzes and added in child CBCL anxiety, depressive, internalizing and externalizing symptoms to ensure that effects were not due to potential differences in symptomatology. To further ensure that the findings were not solely due to differences in maternal depression between groups, we selected the subsample of children whose mothers reported they had ever been depressed and repeated analyzes of prenatal SSRI exposure on BOLD response in the subsample. We also performed analyzes directly comparing three groups: *in utero* SSRI exposed children, children exposed to maternal depression but not SSRIs and unexposed children.

**Statistical analyzes—human study.** Analyzes were performed using R (version 1.4.1717). For descriptive analyzes, chi-square tests were used for categorical variables, and *t*-tests for continuous variables. For regression analysis linear mixed effects models were used using R-package “lme4”. Analyzes were two-tailed and adjusted for multiple comparisons (9 brain regions x 2 hemispheres) with FDR corrections with significance set at  $p_{FDR} < 0.05$ . All continuous variables were standardized, binary variables were not, thus beta values estimate change in standard deviation of the outcome variable between groups (similar to Cohen’s D). All analyzes were weighted by propensity scores to minimize confounding due to differences between mothers who used SSRIs prenatally and mothers who did not (see below). Individual BOLD response values were winsorized to 3 standard deviations from the mean to diminish the influence of spurious outliers. To investigate sex differences, sex was entered into the models as an interaction term. When there was a significant interaction analyzes were also run stratified by sex. Multicollinearity was of no concern with maximum variance inflation factor quantifying any multicollinearity was 3.5 (for behavioral measures on the N-back task), where 1 is the minimum and values of 10 and higher indicate concerning multicollinearity<sup>85</sup>. Removing the behavioral N-back variables from the models did not change the results. Mediation analyzes were performed including covariates and propensity score weighting using R-package “mediation” for causal mediation analysis.

**Propensity score weighting.** We used propensity score weighting to generate balancing weights for causal effect estimation. We used R-package Weightit to balance prenatal covariates between SSRI

exposure and control groups using an ATT (average treatment effect on the treated) estimand. The list of covariates we balanced were the following: knowing of pregnancy use of: alcohol, tobacco, cannabis, caffeine, cocaine/crack cocaine, heroin/morphine, oxycodone, prenatal vitamins, pregnancy illnesses, whether the pregnancy was planned, maternal lifetime depression, maternal age at pregnancy, number of doctors’ visits during pregnancy, mother’s race/ethnicity, maternal education. The resulting propensity scores were used to weight participants for all linear mixed models. These variables were also entered into the linear mixed models in a double robust approach<sup>86</sup>.

**Power analysis.** For each of the mouse data, we based animal numbers on an  $\alpha = 0.05$ , power = 0.80, with variability and effect size from prior data or if those data were not available with a medium/large effect size ( $f = 0.5$ ). In the pharmacological manipulation (perinatal fluoxetine) we assumed at least 30% effect size. Missing data was addressed by appropriate mixed effects models when possible.

For the human data we used data from an existing cohort study. We calculated that we were powered to detect small-medium effect sizes ( $d \sim 0.35$ ) with a power of 80% and medium and large effect sizes ( $d > 0.5$ ) with a power of more than 90%.

## Reporting summary

Further information on research design is available in the Nature Portfolio Reporting Summary linked to this article.

## Data availability

ABCD study data is available for download through [nda.nih.gov](https://nda.nih.gov). Source data are provided with this paper.

## References

- Betts, K. S., Williams, G. M., Najman, J. M. & Alati, R. The relationship between maternal depressive, anxious, and stress symptoms during pregnancy and adult offspring behavioral and emotional problems. *Depress Anxiety* **32**, 82–90 (2015).
- O’connor, T. G., Heron, J. & Glover, V. Antenatal anxiety predicts child behavioral/emotional problems independently of postnatal depression. *J. Am. Acad. Child Adolesc. Psychiatry* **41**, 1470–1477 (2002).
- Field, T., Diego, M. & Hernandez-Reif, M. Prenatal depression effects on the fetus and newborn: a review. *Infant Behav. Dev.* **29**, 445–455 (2006).
- Andrade, S. E. et al. Use of selective serotonin reuptake inhibitors (SSRIs) in women delivering liveborn infants and other women of child-bearing age within the US food and drug administration’s mini-sentinel program. *Arch. Women’s. Ment. Health* **19**, 969–977 (2016).
- Molenaar, N. M. et al. The international prevalence of antidepressant use before, during, and after pregnancy: a systematic review and meta-analysis of timing, type of prescriptions and geographical variability. *J. Affect. Disord.* **264**, 82–89 (2020).
- Hendrick, V. et al. Placental passage of antidepressant medications. *Am. J. Psychiatry* **160**, 993–996 (2003).
- Hermansen, T. K. & Melinder, A. Prenatal SSRI exposure: Effects on later child development. *Child Neuropsychol.* **21**, 543–569 (2015).
- Bérard, A., Zhao, J.-P. & Sheehy, O. Sertraline use during pregnancy and the risk of major malformations. *Am. J. Obstet. Gynecol.* **212**, 795.e1–795.e12 (2015).
- Chambers, C. D., Johnson, K. A., Dick, L. M., Felix, R. J. & Jones, K. L. Birth outcomes in pregnant women taking fluoxetine. *N. Engl. J. Med.* **335**, 1010–1015 (1996).
- Malm, H., Artama, M., Gissler, M. & Ritvanen, A. Selective serotonin reuptake inhibitors and risk for major congenital anomalies. *Obstet. Gynecol.* **118**, 111–120 (2011).

11. Alwan, S. et al. Use of selective serotonin-reuptake inhibitors in pregnancy and the risk of birth defects. *N. Engl. J. Med.* **356**, 2684–2692 (2007).
12. Singal, D. et al. In utero antidepressants and neurodevelopmental outcomes in kindergarteners. *Pediatrics* **145**, e20191157 (2020).
13. Liu, X. et al. Antidepressant use during pregnancy and psychiatric disorders in offspring: danish nationwide register based cohort study. *BMJ* **358**, j3668 (2017).
14. Rommel, A.-S., Bergink, V., Liu, X., Munk-Olsen, T. & Molenaar, N. M. Long-term effects of intrauterine exposure to antidepressants on physical, neurodevelopmental, and psychiatric outcomes: a systematic review. *J. Clin. Psychiatry* **81**, 19r12965 (2020).
15. Bliddal, M. et al. Prenatal antidepressant exposure and emotional disorders until age 22: a danish register study. *Child Adolesc. Psychiatry Ment. Health* **17**, 73 (2023).
16. Suarez, E. A. et al. Association of antidepressant use during pregnancy with risk of neurodevelopmental disorders in children. *JAMA Intern. Med.* **182**, 1149–1160 (2022).
17. Rommel, A.-S. et al. Long-term prenatal effects of antidepressant use on the risk of affective disorders in the offspring: a register-based cohort study. *Neuropsychopharmacology* **46**, 1518–1525 (2021).
18. Rebello, T. J. et al. Postnatal day 2 to 11 constitutes a 5-HT-sensitive period impacting adult mPFC function. *J. Neurosci.* **34**, 12379–12393 (2014).
19. Miceli, S. et al. High serotonin levels during brain development alter the structural input-output connectivity of neural networks in the rat somatosensory layer IV. *Front. Cell. Neurosci.* **7**, 88 (2013).
20. Ansorge, M. S., Zhou, M., Lira, A., Hen, R. & Gingrich, J. A. Early-life blockade of the 5-HT transporter alters emotional behavior in adult mice. *Science* **306**, 879–881 (2004).
21. Li, Q., Wichems, C., Heils, A., Lesch, K.-P. & Murphy, D. L. Reduction in the density and expression, but not G-protein coupling, of serotonin receptors (5-HT1A) in 5-HT transporter knock-out mice: gender and brain region differences. *J. Neurosci.* **20**, 7888–7895 (2000).
22. Linhares, S. S. G. et al. Prenatal exposure to fluoxetine modulates emotionality and aversive memory in male and female rat offspring. *Behav. Pharmacol.* **33**, 575–588 (2022).
23. Persico, A. M. et al. Barrel pattern formation requires serotonin uptake by thalamocortical afferents, and not vesicular monoamine release. *J. Neurosci.* **21**, 6862–6873 (2001).
24. Ansorge, M. S., Morelli, E. & Gingrich, J. A. Inhibition of serotonin but not norepinephrine transport during development produces delayed, persistent perturbations of emotional behaviors in mice. *J. Neurosci.* **28**, 199–207 (2008).
25. Dobbing, J. & Sands, J. Comparative aspects of the brain growth spurt. *Early Hum. Dev.* **3**, 79–83 (1979).
26. Bockhorst, K. H. et al. Early postnatal development of rat brain: in vivo diffusion tensor imaging. *J. Neurosci. Res.* **86**, 1520–1528 (2008).
27. Semple, B. D., Blomgren, K., Gimlin, K., Ferriero, D. M. & Noble-Haesslein, L. J. Brain development in rodents and humans: Identifying benchmarks of maturation and vulnerability to injury across species. *Prog. Neurobiol.* **106–107**, 1–16 (2013).
28. Suri, D., Teixeira, C. M., Caglistro, M. K. C., Mahadevia, D. & Ansorge, M. S. Monoamine-sensitive developmental periods impacting adult emotional and cognitive behaviors. *Neuropsychopharmacology* **40**, 88–112 (2015).
29. Kindt, K. S., Tam, T., Whiteman, S. & Schafer, W. R. Serotonin promotes go-dependent neuronal migration in *Caenorhabditis elegans*. *Curr. Biol.* **12**, 1738–1747 (2002).
30. Azmitia, E. C. Modern views on an ancient chemical: serotonin effects on cell proliferation, maturation, and apoptosis. *Brain Res. Bull.* **56**, 413–424 (2001).
31. Ranzil, S. et al. The relationship between the placental serotonin pathway and fetal growth restriction. *Biochimie* **161**, 80–87 (2019).
32. Baudat, M., de Kort, A. R., van den Hove, D. L. A. & Joosten, E. A. Early-life exposure to selective serotonin reuptake inhibitors: Long-term effects on pain and affective comorbidities. *Eur. J. Neurosci.* **55**, 295–317 (2022).
33. Wollesen, T., Degnan, B. M. & Wanninger, A. Expression of serotonin (5-HT) during CNS development of the cephalopod mollusk, *Idiosepius notoides*. *Cell Tissue Res* **342**, 161–178 (2010).
34. Edsinger, E. & Dölen, G. A conserved role for serotonergic neurotransmission in mediating social behavior in octopus. *Curr. Biol.* **28**, 3136–3142.e4 (2018).
35. Mohammad-Zadeh, L. F., Moses, L. & Gwaltney-Brant, S. M. Serotonin: a review. *J. Vet. Pharmacol. Ther.* **31**, 187–199 (2008).
36. Casey, B. J. et al. The Adolescent Brain Cognitive Development (ABCD) study: imaging acquisition across 21 sites. *Dev. Cogn. Neurosci.* **32**, 43–54 (2018).
37. King, J. A. et al. Procedure for minimizing stress for fMRI studies in conscious rats. *J. Neurosci. Methods* **148**, 154–160 (2005).
38. Ferris, C. F. et al. Studies on the Q175 knock-in model of huntington's disease using functional imaging in awake mice: evidence of olfactory dysfunction. *Front. Neurol.* **5**, 94 (2014).
39. Koc, D. et al. Prenatal antidepressant exposure and offspring brain morphologic trajectory. *JAMA Psychiatry* **80**, 1208–1217 (2023).
40. Malm, H. et al. Gestational exposure to selective serotonin reuptake inhibitors and offspring psychiatric disorders: a national register-based study. *J. Am. Acad. Child Adolesc. Psychiatry* **55**, 359–366 (2016).
41. Hammen, C. & Brennan, P. A. Severity, chronicity, and timing of maternal depression and risk for adolescent offspring diagnoses in a community sample. *Arch. Gen. Psychiatry* **60**, 253–258 (2003).
42. van Dijk, M. T., Murphy, E., Posner, J. E., Talati, A. & Weissman, M. M. Association of multigenerational family history of depression with lifetime depressive and other psychiatric disorders in children: results from the Adolescent Brain Cognitive Development (ABCD) study. *JAMA Psychiatry* **78**, 778–787 (2021).
43. Silva, B. A., Gross, C. T. & Gräff, J. The neural circuits of innate fear: detection, integration, action, and memorization. *Learn. Mem.* **23**, 544–555 (2016).
44. Staples, L. G. Predator odor avoidance as a rodent model of anxiety: learning-mediated consequences beyond the initial exposure. *Neurobiol. Learn. Mem.* **94**, 435–445 (2010).
45. Lugo-Candelas, C. et al. Associations between brain structure and connectivity in infants and exposure to selective serotonin reuptake inhibitors during pregnancy. *JAMA Pediatr.* **172**, 525–533 (2018).
46. Mukhopadhyay, S., Chatterjee, A., Tiwari, P., Ghai, U. & Vaidya, V. A. Postnatal fluoxetine treatment alters perineuronal net formation and maintenance in the hippocampus. *eNeuro* **8** <https://doi.org/10.1523/eneuro.0424-20.2021> (2021).
47. Karpova, N. N., Lindholm, J., Pruunsild, P., Timmusk, T. & Castrén, E. Long-lasting behavioural and molecular alterations induced by early postnatal fluoxetine exposure are restored by chronic fluoxetine treatment in adult mice. *Eur. Neuropsychopharmacol.* **19**, 97–108 (2009).
48. Unroe, K. A., Glover, M. E., Shupe, E. A., Feng, N. & Clinton, S. M. Perinatal SSRI exposure disrupts G protein-coupled receptor BA13 in developing dentate gyrus and adult emotional behavior: relevance to psychiatric disorders. *Neuroscience* **471**, 32–50 (2021).
49. Menezes, E. C. et al. Reduced motivation in perinatal fluoxetine-treated mice: a hypodopaminergic phenotype. *J. Neurosci.* **41**, 2723–2732 (2021).
50. Hutchison, S. M., Mâsse, L. C., Pawlusk, J. L. & Oberlander, T. F. Perinatal selective serotonin reuptake inhibitor (SSRI) and other antidepressant exposure effects on anxiety and depressive



- behaviors in offspring: A review of findings in humans and rodent models. *Reprod. Toxicol.* **99**, 80–95 (2021).
51. Bloodgood, D. W., Sugam, J. A., Holmes, A. & Kash, T. L. Fear extinction requires infralimbic cortex projections to the basolateral amygdala. *Transl. Psychiatry* **8**, 60 (2018).
  52. Yu, W. et al. Prenatal selective serotonin reuptake inhibitor (SSRI) exposure induces working memory and social recognition deficits by disrupting inhibitory synaptic networks in male mice. *Mol. Brain* **12**, 29 (2019).
  53. Giustino, T. F. & Maren, S. The role of the medial prefrontal cortex in the conditioning and extinction of fear. *Front. Behav. Neurosci.* **9**, 298 (2015).
  54. Gross, C., Santarelli, L., Brunner, D., Zhuang, X. & Hen, R. Altered fear circuits in 5-HT1A receptor KO mice. *Biol. Psychiatry* **48**, 1157–1163 (2000).
  55. Gaspar, P., Cases, O. & Maroteaux, L. The developmental role of serotonin: news from mouse molecular genetics. *Nat. Rev. Neurosci.* **4**, 1002–1012 (2003).
  56. Okaty, B. W., Commons, K. G. & Dymecki, S. M. Embracing diversity in the 5-HT neuronal system. *Nat. Rev. Neurosci.* **20**, 397–424 (2019).
  57. Hale, M. W. & Lowry, C. A. Functional topography of midbrain and pontine serotonergic systems: implications for synaptic regulation of serotonergic circuits. *Psychopharmacology* **213**, 243–264 (2011).
  58. Jacobs, B. L. & Azmitia, E. C. Structure and function of the brain serotonin system. *Physiol. Rev.* **72**, 165–229 (1992).
  59. Kiyasova, V. et al. A genetically defined morphologically and functionally unique subset of 5-HT neurons in the mouse raphe nuclei. *J. Neurosci.* **31**, 2756–2768 (2011).
  60. Kredlow, M. A. et al. Prefrontal cortex, amygdala, and threat processing: implications for PTSD. *Neuropsychopharmacology* **47**, 247–259 (2022).
  61. Stein, M. B., Simmons, A. N., Feinstein, J. S. & Paulus, M. P. Increased amygdala and insula activation during emotion processing in anxiety-prone subjects. *Am. J. Psychiatry* **164**, 318–327 (2007).
  62. Liu, W.-J. et al. Abnormal functional connectivity of the amygdala-based network in resting-state fMRI in adolescents with generalized anxiety disorder. *Med. Sci. Monit.* **21**, 459–467 (2015).
  63. Williams, L. M. et al. Amygdala reactivity to emotional faces in the prediction of general and medication-specific responses to antidepressant treatment in the randomized iSPOT-D trial. *Neuropsychopharmacology* **40**, 2398–2408 (2015).
  64. Rotem-Kohavi, N., Williams, L. J. & Oberlander, T. F. Advanced neuroimaging: a window into the neural correlates of fetal programming related to prenatal exposure to maternal depression and SSRIs. *Semin. Perinatol.* **44**, 151223 (2020).
  65. Rotem-Kohavi, N. et al. Alterations in resting-state networks following in utero selective serotonin reuptake inhibitor exposure in the neonatal brain. *Biol. Psychiatry Cogn. Neurosci. Neuroimaging* **4**, 39–49 (2019).
  66. Isosaka, T. et al. Htr2a-expressing cells in the central amygdala control the hierarchy between innate and learned fear. *Cell* **163**, 1153–1164 (2015).
  67. Matsuo, T. et al. Artificial hibernation/life-protective state induced by thiazoline-related innate fear odors. *Commun. Biol.* **4**, 101 (2021).
  68. Wang, Y. et al. Large-scale forward genetics screening identifies *Trpa1* as a chemosensor for predator odor-evoked innate fear behaviors. *Nat. Commun.* **9**, 2041 (2018).
  69. Mathis, A. et al. DeepLabCut: markerless pose estimation of user-defined body parts with deep learning. *Nat. Neurosci.* **21**, 1281–1289 (2018).
  70. Akiti, K. et al. Striatal dopamine explains novelty-induced behavioral dynamics and individual variability in threat prediction. *Neuron* **110**, 3789–3804.e9 (2022).
  71. Ferris, C. F. Applications in awake animal magnetic resonance imaging. *Front. Neurosci.* **16**, 854377 (2022).
  72. Mandino, F., Vujic, S., Grandjean, J. & Lake, E. M. R. Where do we stand on fMRI in awake mice? *Cereb. Cortex* **34** (2024).
  73. Sadaka, A. H. et al. Cannabidiol has a unique effect on global brain activity: a pharmacological, functional MRI study in awake mice. *J. Transl. Med.* **19**, 220 (2021).
  74. Bhattacharyya, P. K., Phillips, M. D., Stone, L. A. & Lowe, M. J. Activation volume vs BOLD signal change as measures of fMRI activation – Its impact on GABA – fMRI activation correlation. *Magn. Reson. Imaging* **42**, 123–129 (2017).
  75. Kenkel, W. M. et al. Functional magnetic resonance imaging in awake transgenic fragile X rats: evidence of dysregulation in reward processing in the mesolimbic/habenular neural circuit. *Transl. Psychiatry* **6**, e763 (2016).
  76. Brevard, M. E., Duong, T. Q., King, J. A. & Ferris, C. F. Changes in MRI signal intensity during hypercapnic challenge under conscious and anesthetized conditions. *Magn. Reson. Imaging* **21**, 995–1001 (2003).
  77. Friston, K. J. et al. Statistical parametric maps in functional imaging: A general linear approach. *Hum. Brain Mapp.* **2**, 189–210 (1994).
  78. Buxton, R. B., Wong, E. C. & Frank, L. R. Dynamics of blood flow and oxygenation changes during brain activation: the balloon model. *Magn. Reson. Med.* **39**, 855–864 (1998).
  79. Genovese, C. R., Lazar, N. A. & Nichols, T. Thresholding of statistical maps in functional neuroimaging using the false discovery rate. *Neuroimage* **15**, 870–878 (2002).
  80. Genovese, C. & Wasserman, L. Operating characteristics and extensions of the false discovery rate procedure. *J. R. Stat. Soc.* (2002).
  81. Benjamini, Y. & Hochberg, Y. Controlling the false discovery rate: a practical and powerful approach to multiple testing. *J. R. Stat. Soc.* **57**, 289–300 (1995).
  82. Hagler, D. J. et al. Image processing and analysis methods for the adolescent brain cognitive development study. *Neuroimage* **202**, 116091 (2019).
  83. Cox, R. W. AFNI: software for analysis and visualization of functional magnetic resonance neuroimages. *Comput. Biomed. Res.* **29**, 162–173 (1996).
  84. Chaarani, B. et al. Baseline brain function in the preadolescents of the ABCD Study. *Nat. Neurosci.* **24**, 1176–1186 (2021).
  85. Alin, A. et al. Multicollinearity. *Wiley Interdisciplinary Rev.: Comput. Stat.* **2**, 370–374 (2010).
  86. Funk, M. J. et al. Doubly robust estimation of causal effects. *Am. J. Epidemiol.* **173**, 761–767 (2011).

## Acknowledgements

We would like to thank members of the Ansorge's lab for methodological and conceptual discussions. This work was supported by an AFSP Young Investigator Award YIG-R-001-19 (MvD), Depression Center Pilot Award from the Columbia Department of Psychiatry (AT), Sackler Institute for Developmental Psychobiology (GZ), 1K01MH131895-01A1 (GZ), R01MH099118 (MSA), Sackler Institute for Developmental Psychobiology (MSA), R01MH036197 (MMW). The content is solely the responsibility of the authors and does not necessarily represent the official views of the National Institutes of Health or of any other sponsor.

## Author contributions

G.Z., M.S.A., M.C.C., M.T.v.D., A.T., J.A.G., C.F., and M.M.W. conceived and supervised all aspects of the study. G.Z. and M.C.C. performed behavioral and imaging experiments in mice. A.S.M. assisted with mouse



behavior. M.T.v.D. performed behavioral and imaging assessment of human ABCD data. G.Z. and M.T.v.D. wrote the manuscript. A.L.K. and N.P. assisted with Matlab script for Deeplabcut analysis of behavior. A.L.R. and A.L.K. assisted with data curation and analysis. C.F., M.C.C., and P.K. performed and analyzed brain imaging experiments in mice. P.S. and K.I. performed Deeplabcut analysis of behavior. C.L.C. and P.D.G. contributed conceptually to the human study design. G.Z. and M.T.v.D. contributed equally and have the right to list their name first in their C.V., M.S.A., and J.A.G. share last authorship. All authors contributed to the article and approved the submitted version.

## Competing interests

MMW has received royalties from Oxford University Press, Perseus Books Group, American Psychiatric Association Publishing, and Multi-Health Systems. CFF has a financial interest in Animal Imaging Research, a company that makes radiofrequency electronics and holders for awake animal imaging. CFF and PK have a partnership interest in Ekam Solutions, a company that develops 3D MRI atlases for animal research. None of these present any conflict with the present work. The remaining authors declare no competing interests.

## Additional information

**Supplementary information** The online version contains supplementary material available at <https://doi.org/10.1038/s41467-025-58785-4>.

**Correspondence** and requests for materials should be addressed to Mark S. Ansorge.

**Peer review information** *Nature Communications* thanks the anonymous reviewers for their contribution to the peer review of this work. A peer review file is available.

**Reprints and permissions information** is available at <http://www.nature.com/reprints>

**Publisher's note** Springer Nature remains neutral with regard to jurisdictional claims in published maps and institutional affiliations.

**Open Access** This article is licensed under a Creative Commons Attribution-NonCommercial-NoDerivatives 4.0 International License, which permits any non-commercial use, sharing, distribution and reproduction in any medium or format, as long as you give appropriate credit to the original author(s) and the source, provide a link to the Creative Commons licence, and indicate if you modified the licensed material. You do not have permission under this licence to share adapted material derived from this article or parts of it. The images or other third party material in this article are included in the article's Creative Commons licence, unless indicated otherwise in a credit line to the material. If material is not included in the article's Creative Commons licence and your intended use is not permitted by statutory regulation or exceeds the permitted use, you will need to obtain permission directly from the copyright holder. To view a copy of this licence, visit <http://creativecommons.org/licenses/by-nc-nd/4.0/>.

© The Author(s) 2025